Aberystwyth University

Holocene dynamics of the Southern Hemisphere westerly winds and possible links to CO2 outgassing

Saunders, Krystyna ; Roberts, Stephen J.; Perren, Bianca; Butz, Christoph; Sime, Louise; Davies, Sarah; Van Nieuwenhuyze, Wim; Grosjean, Martin; Hodgson, Dominic A.

1   **Holocene dynamics of the Southern Hemisphere westerly winds and links to CO₂ outgassing**

2

3   Krystyna M. Saunders*[1,2], Stephen J. Roberts[3], Bianca Perren[3], Christoph Butz[1],

4   Louise Sime[3], Sarah Davies[4], Wim Van Nieuwenhuyze [5], Martin Grosjean[1], Dominic A.

5   Hodgson[3,6]

6

7   [1]Institute of Geography and Oeschger Centre for Climate Change Research, University of Bern,

8   Bern, Switzerland; [2]Australian Nuclear Science and Technology Organisation, Sydney, Australia;

9   [3]British Antarctic Survey, Cambridge, UK; [4]Department of Geography and Earth Sciences,

10   Aberystwyth University, Aberystwyth, UK; [5]Department of Biology, University of Ghent,

11   Belgium; [6]Department of Geography, University of Durham, UK

12

13   *Corresponding author. KS. krystyna.saunders@ansto.gov.au

14

15   **The Southern Hemisphere westerly winds (SHW) play a significant role in regulating the**

16   **capacity of the Southern Ocean carbon sink. They modulate upwelling of carbon-rich deep**

17   **water and, with sea ice, determine the ocean surface area available for air-sea gas exchange.**

18   **Some models suggest the current strengthening and poleward shift of the SHW will weaken**

19   **the carbon sink. If correct, centennial- to millennial-scale reconstructions of SHW intensity**

20   **should be linked with past changes in atmospheric CO₂, temperature, and sea ice. Here, we**

21   **present a 12,300-year reconstruction of wind strength based on three independent proxies**

22   **that track inputs of sea salt aerosols and minerogenic particles accumulating in lake**

23 **sediments on sub-Antarctic Macquarie Island. Between c. 12.1–11.2 ka BP and since c. 7 ka**

24 **BP, wind intensities were above their long-term mean, and corresponded with increasing**

25 **atmospheric CO_2. Conversely, from c. 11.2–7.2 ka BP, wind intensities were below their long-**

26 **term mean and corresponded with decreasing atmospheric CO_2. These observations are**

27 **consistent with model inferences of enhanced SHW contributing to the long-term outgassing**

28 **of CO_2 from the Southern Ocean.**

29

30 The Southern Ocean currently accounts for 43 ± 3% of the global oceanic anthropogenic CO_2

31 uptake [1] mitigating (perhaps temporarily) the climatic effects of enhanced greenhouse gases in

32 the atmosphere. The capacity of the Southern Ocean to absorb CO_2 at the surface is

33 determined by the balance between processes sequestering carbon (e.g., diffusion and the

34 biological carbon pump) versus processes releasing old carbon from the deep ocean to the

35 atmosphere (e.g., upwelling and outgassing) [2,3]. Attempts to model these processes have

36 yielded conflicting results. One model based on instrumental data collected between 1981 and

37 2004 suggested that the Southern Ocean carbon sink has weakened [4]. Conversely, analyses of

38 the same data extended to 2011 suggest a reinvigoration of the carbon sink since 2002 [5]. This

39 latter trend is also seen in measurements of the difference between the partial pressure of CO_2

40 in ocean surface water and the overlying atmosphere (ΔpCO_2) of the Southern Ocean in Drake

41 Passage [6]. Spatial extrapolation of the relatively few pCO_2 measurements from the Southern

42 Ocean as a whole suggests a trend towards a weakening sink in the 1990s, but a strengthening

43 one in the 2000s [7].

44

45   One of the main drivers of the Southern Ocean CO_2 sink are the Southern Hemisphere westerly

46   winds (SHW), which are strongest from 50-55°S over the Southern Ocean [8] (Fig. 1a). Changes in

47   the SHW are mainly determined by atmospheric temperature gradients, sea surface

48   temperature and regional sea ice [9]. In turn they influence ocean circulation [10,11], regulate sea

49   ice extent [12] and control the upwelling of dissolved inorganic carbon-rich deep water to

50   Antarctic surface waters [2]. All are processes that modulate the net uptake of CO_2 by the ocean

51   from the atmosphere [13]. Studies that propose a weakening of the Southern Ocean CO_2 sink

52   attribute it to the recent strengthening and poleward shift of the SHW resulting from changes

53   in surface temperature gradients due to human activities, including ozone depletion [4]. This has

54   brought carbon-rich waters to the surface ocean and reduced ΔpCO_2 [1].

55

56   Despite the potential importance of the SHW in modulating net uptake of CO_2 by the Southern

57   Ocean, recent extrapolations of the future behaviour of the CO_2 sink are solely based on short-

58   term instrumental records and low spatial and temporal measurements of ΔpCO_2 [4,5]. If current

59   theories regarding a potential weakening of the CO_2 sink are correct, past reconstructions of

60   changes in the intensity of the SHW over the Southern Ocean should show clear links between

61   atmospheric CO_2, temperature and sea ice over longer (centennial-millennial) time scales.

62

63   To date, palaeoclimatic reconstructions of the SHW derive mostly from southernmost South

64   America, the only continental landmass intersecting the mid to northern core of the SHW.

65   However, they 'do not provide a consistent picture of the SHW during the Holocene' [(14, p.14)].

66   This can be partly attributed to a reliance on proxies of past changes in effective precipitation

67   and/or temperature to infer changes in wind strength. Examples include sub-fossil pollen

68   assemblages in peat and lake sediment cores (e.g., [15,16]), geochemical proxies of the

69   precipitation-evaporation balance (e.g., [17]), and rainfall changes influencing runoff into fjord [18]

70   and ocean [19] sediments. The application of proxies that measure windblown transport (e.g.,

71   exotic pollen [20,21], dust [22]) are rare, and their relationship to wind strength not always

72   straightforward [14].

73

74   Avoiding continental landmasses with complex orographic effects, and applying multi-proxy

75   (and independent) methods to track past changes in wind intensity circumvents these issues.

76   The latter tests whether different wind proxies record congruent patterns in the direction and

77   relative magnitude of change, providing a validation that the proxies are responding to the

78   external forcing of the SHW rather than local or internal dynamics at the study site.

79

80   We carried out a detailed reconstruction of Holocene changes in SHW intensity at sub-Antarctic

81   Macquarie Island. The first aim was to reconstruct changes in the dynamics and relative

82   strength of the SHW over the core jets of the Antarctic Circumpolar Current; the region most

83   relevant to Southern Ocean air-sea gas exchange [23]. The second was to test which of the

84   competing models of a weakening [4] or reinvigoration [5] of the carbon sink in recent decades is

85   supported by the long-term palaeo-record. We did not consider changes in the position of the

86   SHW core belt (50-55°S) in detail. More well-dated, multi proxy records are needed from

87   broader latitudinal and longitudinal ranges to reliably separate changes in intensity from

88   changes in latitudinal position.

89

Sub-Antarctic Macquarie Island

90

91 Macquarie Island is a small, 130 km^2, sub-Antarctic island located a few hundred kilometres

92 north of the Polar Front (54°S, 158°E; Fig. 1 and Supplementary Note 1). The sub-Antarctic

93 islands are the only landmasses, other than southernmost South America, that lie in the core of

94 the SHWs. Macquarie Island experiences mean annual wind speeds of ~35 km hr^{-1}, a mean daily

95 wind run of 751 km, gusts of up to 185 km hr^{-1} [24] and its climate is representative of the core

96 belt of the SHW (Fig. 1 c, d). Wind almost exclusively comes from the west-northwest

97 (Supplementary Figs. 2 and 3). This results in strong west to east gradients in sea-spray [25] and

98 minerogenic wind-blown aerosols being deposited across the island. These aerosols accumulate

99 over time in lake and peat sediments, preserving a record of relative changes in SHW intensity,

100 with periods of more (or less) sea spray or deposited minerogenic material reflecting phases of

101 stronger (or weaker) winds. We applied a combination of three methods to reconstruct past

102 changes in SHW intensity using a sedimentary sequence from Emerald Lake, a small lake

103 perched on the western edge of the Macquarie Island plateau, and directly exposed to westerly

104 air flow (Supplementary Note 2). The sediment sequence was radiometrically dated with 44 ^{14}C

105 and 11 ^{210}Pb dates (Supplementary Note 3). Freshwater diatom-based inference models

106 provided a measure of past sea spray aerosol inputs through their effect on the conductivity

107 and diatom species assemblages in lakes [25]. These were compared with two independent

108 measures of minerogenic aerosol inputs based on micro X-ray fluorescence (μ-XRF) core

109 scanning and hyperspectral imaging. These proxies, and the sedimentology of the core, are

110 described in Supplementary Notes 4, 5.

111

Holocene dynamics of the SHW

113   The three proxies used in the present study show similar patterns in wind strength over

114   Macquarie Island over the last c. 12.3 ka BP (Fig. 2, Supplementary Note 5). The strongest

115   correlation is between the two methods measuring minerogenic inputs (r=0.85, p <0.0001,

116   Supplementary Table 4). These are also significantly correlated with the independent diatom-

117   inferred conductivity / sea spray proxy (r=0.56 and r=0.65, p <0.0001). The slightly weaker

118   correlations with the diatom-inferred conductivity / sea spray proxy can be attributed to lake

119   water nutrients and pH which explain smaller yet independent portions of the variance in the

120   diatom data [25]. The correlations between the minerogenic wind proxies and diatom-inferred

121   conductivity excludes changes in dust supply from source regions as a major factor modifying

122   the reconstructions. The period from 7.5–7.2 ka BP shows a negative correlation between the

123   minerogenic proxies and diatom-inferred conductivity. Based on the presence of sub-aerial

124   diatoms, this was attributed to a brief period of low water levels (see Supplementary Note 4).

125

126   In general, the proxies show high relative wind intensity (defined here as periods when at least

127   two of the three wind proxies have values greater than the 95% upper bound of their mean,

128   Supplementary Table 6) between 12.1–11.2, 9.2–8.5, 7.9–7.7, 7.0–5.6, 5.3–0.2 and 0.1–0 ka BP.

129   Low relative wind intensities were recorded from 11.2–9.2, 8.4–7.9, 7.7–7.0 and 0.2–0.1 ka BP.

130   The key features are high relative winds spanning the end of the Last Glacial-Interglacial

131   Transition (LGIT) to the early Holocene (12.1–11.2 ka BP), low relative winds during the early

132   Holocene Thermal Maximum (11.2–9.2 ka BP), increased winds and higher amplitude changes

133   between 9.2–5.3 ka BP, and a period of sustained relatively intense winds from 5.3 to 0.2 ka BP

134   (although the resolution of the record is lower during this period) (Fig. 2). After 0.2 ka BP the

135   wind intensity drops and then increases in the most recent decades.

136

137   **SHW dynamics, atmospheric CO_2, sea ice and temperature**

138   Significant correlations between the three independent wind proxies support the hypothesis

139   that, together, they provide a reliable record of changes in the dynamics of the SHW in their

140   core belt, and more specifically at Macquarie Island. Therefore, to address our wider objective

141   of evaluating the role of the SHW as a driver of natural CO_2 variations, we compared past

142   changes in the SHW at Macquarie Island with other hemispheric changes in the ocean and

143   atmosphere. These include far-field proxy records in the EPICA Dome C ice core of sea ice (sea

144   salt Na+ aerosol flux)[26], temperature and CO_2[2], and marine core microfossil-based

145   measurements of winter sea ice concentration (WSI %) in selected (and not necessarily

146   representative) marine cores from the South Atlantic (PS2090[27]) and South Pacific sector near

147   Macquarie Island (E27-23[28], Fig. 3).

148

149   *12.1–11.2 ka BP:* The end of the LGIT and early Holocene are characterised by intense SHW.

150   Many records at similar latitudes in southernmost South America (Supplementary Fig. 15c-e),

151   and elsewhere in the Southern Hemisphere (Supplementary Note 7) agree. This period of

152   intense SHW is accompanied by marked increases in atmospheric CO_2 and temperature (Fig 3e,

153   f), and declines in sea ice (Fig. 3c, d). There are both proxy and model-based studies that

154   support the magnitude and direction of these changes across the LGIT [10,29,30]. Specifically, the

155   persistent winds identified here are consistent with enhanced Southern Ocean upwelling [10]

156   accounting for at least part of the deglacial rise in atmospheric CO_2, and accompanied by

157   increases in atmospheric [30] and sea surface temperatures [29]. Temporal patterns in our records

158   are also consistent with the retreat of sea ice having a positive feedback on the ocean surface

159   area available for the outgassing of CO_2 [29] (Fig. 3).

160

161   *11.2–9.2 ka BP:* An early Holocene Thermal Maximum between 11.2–9.2 ka BP is clearly

162   resolved in Antarctica [31] and other records across the Southern Hemisphere, including the

163   western side of the Andes from 49–55°S [14]. This reduced the thermal gradient between the mid

164   and high latitudes and resulted in persistent low intensity winds at Macquarie Island (Fig. 3a, b).

165   This is consistent with selected records from South America [32,33], Tasmania and New Zealand [32]

166   (Supplementary Note 7), and a reduced thermal gradient in the Southern Ocean east and south

167   of New Zealand [34]. If replicated in further studies, this would suggest a widespread decrease in

168   wind intensity across the Southern Hemisphere from 41°S to 54°S (Macquarie Island, see

169   Supplementary Note 7). The sustained warm conditions and low wind intensity during this

170   period corresponded with reduced sea ice in marine [27,29] and ice core records [35], and was

171   followed by the only long-term decline in atmospheric CO_2 (c. 10.5–7.2 ka BP) since the

172   Antarctic Cold Reversal [36].

173

174   *9.2–5.3 ka BP:* All three wind proxies at Emerald Lake show a period of increased and higher

175   amplitude changes in wind intensity (relative to the early Holocene Thermal Maximum),

176   punctuated by relatively shorter lived (multi-centennial) periods when wind strength is

177   significantly lower. This corresponds to some terrestrial records of enhanced precipitation in

178   South America (e.g., Tamar Lake [32] and Lago Cipreses [33], but not others [8]; see Supplementary

179   Note 7). These increased winds coincide with a downturn in temperature and increases in sea

180   ice (Fig. 3c, d). During the first part of this period the positive relationship between enhanced

181   winds and sea ice appears similar to the beginning of the record (12.1–11.2 ka BP), but differs,

182   at least until 7 ka BP, because the winds did not correspond with an increase in atmospheric

183   CO_2 (Fig. 3f). We attribute this to the concurrent development of alternative carbon sinks in the

184   terrestrial biosphere, including mineral soils, peat and permafrost carbon [37,38]. However, after

185   7 ka BP, increased wind strength and sea ice correspond to the onset of the steady increase in

186   atmospheric CO_2 that characterised the middle and late Holocene.

187

188   ***5.3–0 ka BP:*** This period of relatively constant and intense winds at Macquarie Island and

189   elevated rainfall inferred from several studies on the western side of the Andes (see

190   Supplementary Note 7, Supplementary Fig 15) corresponds with: relatively high sea ice in the

191   Atlantic sector (Fig. 3c); increases in the ice core ssNa after 4 ka (Fig. 3d); a sustained increase in

192   atmospheric CO_2 (Fig. 3f). Combined, this evidence implies that persistent strong winds led to

193   net Southern Ocean outgassing during the latter part of the Holocene. Over the last 0.2 ka BP,

194   our record of Ti aerosol inputs into Emerald Lake show an initial decline, followed by an

195   increase in the last c. 100 years. The latter is consistent with instrumental records from

196   Macquarie Island, and other areas of the Southern Ocean, which have shown an intensification

197   and southward shift in the main wind belt [5] (Supplementary Fig. 2). However, during this period,

198   all proxies are potentially compromised by erosional inputs associated with the activities of

199   introduced species [39] ('rabbit-influenced zone'; Fig. 2).

200

201   **SHW, CO$_2$, temperature and sea ice**

202   To develop our understanding of Southern Hemisphere climate dynamics, we now focus on the

203   centennial to millennial relationships between the SHW, atmospheric CO$_2$, temperature and sea

204   ice, and the extent to which they are replicated in selected Global Climate Models.

205

206   First, the Macquarie record shows significant positive relationships between SHW and sea ice

207   particularly through the late LGIT and early Holocene, and possibly during the period of

208   sustained relatively intense winds from 5.3 to 0.2 ka BP (Supplementary Table 4,

209   Supplementary Note 5). This is consistent with CMIP5 models that show significant

210   relationships between SHW jet strength and sea ice area [40]. It has been suggested that a

211   strengthened SHW jet leads to increased Ekman upwelling bringing cooler subsurface water to

212   the surface and strengthened equatorward transport, which is conducive to increased sea ice [12].

213   Alternatively, at least part of the correspondence between the SHW reconstruction and ice core

214   ssNA could be attributed to direct wind-driven transport of ssNa to the Dome C ice core site,

215   independent of changes in sea ice extent, although this has previously been questioned based

216   on chemical signatures in the ice [41]. Thus, except for the 9.2–7 ka BP period, where the

217   relationship is less clear, the Macquarie Island record suggests that, at centennial to millennial

218   timescales during the Holocene, sea ice and the intensity of the SHW were broadly in phase.

219

220　Second, in terms of the relationship between the SHW and atmospheric temperature and CO_2,

221　the Macquarie Island proxy records show that windier periods (i.e., greater than the 95% upper

222　bound of their long-term mean) correspond with periods of increasing atmospheric CO_2 (orange

223　boxes in Fig. 3b, f) from 12.1–11.2 ka BP, and in the last 7 ka. Conversely, the period of lower

224　than mean winds from 11.2 ka BP corresponds with decreasing atmospheric CO_2 (blue boxes in

225　Fig. 3b, f), and a downturn in temperature (Fig. 3e), which persisted until c. 8 ka BP. This

226　relationship is reproduced in short term CMIP5 model experiments, which consistently show a

227　poleward shift and strengthening of the SHW jet in response to increasing greenhouse gases

228　and stratospheric ozone [42]. These observations are consistent with enhanced wind driven

229　upwelling of CO_2 rich deep ocean waters, accounting for at least part of the increase in

230　atmospheric CO_2 across the LGIT and into the early Holocene [3] and the last 7ka, whilst periods

231　of reduced wind strength enhance the Southern Ocean CO_2 sink. The larger magnitude of the

232　increase in CO_2 during the late LGIT and early Holocene (Fig. 3) can be attributed to the higher

233　CO_2 available for release from the glacial deep ocean [43]. In contrast, the moderate increases in

234　CO_2 since 7 ka BP can be attributed to less CO_2 available for release from the ocean and the

235　development of terrestrial carbon sinks [37].

236

237　**SHW and the future of the Southern Ocean carbon sink**

238　Our new records of the SHW, which are aligned with the core jets of the present-day Antarctic

239　Circumpolar Current, suggest large changes in wind intensity over the last 12.1 ka BP. This is in

240　marked contrast to model simulations of the SHW across the Last Glacial termination and

241　Holocene which simulate only relatively small wind speed anomalies (± 1 m s^{-1}) [9,23,44,45]. The

242   correspondence between strong and persistent SHW and the rise in CO_2 during the latter part

243   of the LGIT into the early Holocene, and from 7 ka BP suggests that the winds have contributed

244   to the long-term outgassing of CO_2 from the ocean during these periods. This provides a longer-

245   term perspective on the 30-year instrumental record of ΔpCO_2 and SHW strength, which has

246   been used to evaluate short-term changes in the behaviour of the Southern Ocean carbon sink

247   [4,5]. Specifically, the palaeo-data support the Le Quéré model [4], which suggests a wind-driven

248   weakening of the Southern Ocean carbon sink (enhanced outgassing) prior to 2007 CE as the

249   dominant process. It does not support the alternative Landschützer model [5], which proposes

250   that a stabilisation of the surface waters has counteracted the wind induced upwelling and

251   reinvigorated the carbon sink during the last decade. Therefore, over multi-decadal to

252   millennial timescales, further increases in wind strength will lead to faster accumulation of CO_2

253   in the atmosphere.

254

255   **Methods**

256   A series of lake sediment cores dating back to c. 12.1 ka BP were extracted from Emerald Lake

257   on the western edge of the Macquarie Island plateau. Perched within a small catchment,

258   Emerald Lake is ideally situated to record changes in sea salt and mineral aerosol inputs

259   (Supplementary Notes 2, 3). We applied three independent methods to reconstruct past

260   changes in SHW intensity (Supplementary Note 5). First, to reconstruct past sea salt aerosol

261   inputs, we developed a method to track past changes in lake water conductivity (a function of

262   sea salt aerosol input) using diatom-based inference models [25,46]. These utilise the strong

263   statistical relationship between modern diatom species assemblages and lake water

264 conductivity (weighted averaging partial least squares, two components; $r^2 = 0.92$, $r^2_{jack} = 0.72$,

265 RMSEP = 230 µS cm^{-1} (Supplementary Note 5), which is applied as a transfer function to

266 reconstruct past changes in conductivity from subfossil species assemblages preserved in lake

267 sediments. Second, ITRAX^{TM} micro X-ray fluorescence (µ-XRF) core scanner data were used to

268 track inputs of minerogenic aerosols into the lake, focusing on titanium (Ti), one of the most

269 widely used indicator elements for increased allochthonous inputs [47] from distal and proximal

270 sources [48]. Third, cores were scanned using a Specim hyperspectral camera, which measures

271 reflected optical properties between wavelengths from 400–1000 nm [49]. The ratio of

272 reflectance between 850 and 900 nm (R_{850}/R_{900}) was used as an additional indicator of

273 minerogenic inputs. Statistical analyses of the proxies were undertaken using R 2.15.2 (R

274 Foundation for Statistical Computing), MATLAB® (Supplementary Note 3 for details) and in

275 Sigmaplot v13, using original and 100-year interval 2nd order polynomial LOESS (Local tricube

276 weighting and polynomial regression) smoothing. The calibration and performance of each of

277 these methods together with details of core sedimentology and chronology are described in

278 Supplementary Notes 3, 4 and 5. Potential influences on the proxies (e.g., lake ice cover and

279 relative sea level) are described in Supplementary Note 6.

280

281 **Data Availability**

282 All data are archived at the Australian Antarctic Data Centre (https://data.aad.gov.au/) and

283 Natural Environment Research Council Polar Data Centre (https://www.bas.ac.uk/data/uk-pdc/).

284

285 **References**

286

287   1   Mikaloff-Fletcher, S. E. CLIMATE. An increasing carbon sink? *Science* **349**, 1165,

288   doi:10.1126/science.aad0912 (2015).

289   2   Hodgson , D. A. & Sime, L. C. Southern westerlies and CO_2. *Nat. Geosci.* **3**, 666-667,

290   doi:610.1038/ngeo1970 (2010).

291   3   Toggweiler, J. R., Russell, J. L. & Carson, S. R. Midlatitude westerlies, atmospheric CO2,

292   and climate change during the ice ages. *Palaeoceanography* **21** PA2005

293   doi:10.1029/2005PA001154 (2006).

294   4   Le Quéré, C. *et al.* Saturation of the Southern Ocean CO2 Sink Due to Recent Climate

295   Change. *Science* **316**, 1735 - 1738 (2007).

296   5   Landschützer, P. *et al.* The reinvigoration of the Southern Ocean carbon sink. *Science*

297   **349**, 1221-1224, doi:10.1126/science.aab2620 (2015).

298   6   Munro, D. R. *et al.* Recent evidence for a strengthening CO_2 sink in the Southern Ocean

299   from carbonate system measurements in the Drake Passage (2002–2015). *Geophys. Res.*

300   *Lett.* **42**, 2015GL065194, doi:10.1002/2015GL065194 (2015).

301   7   Ritter, R. *et al.* Observation-Based Trends of the Southern Ocean Carbon Sink. *Geophys.*

302   *Res. Lett.* **44**, 12,339-312,348, doi:doi:10.1002/2017GL074837 (2017).

303   8   Lamy, F. *et al.* Holocene changes in the position and intensity of the Southern Westerly

304   wind belt. *Nat. Geosci.* **3**, 695-699 (2010).

305   9   Sime, L. C. *et al.* Southern Hemisphere westerly wind changes during the Last Glacial

306   Maximum: model-data comparison. *Quaternary Sci. Rev.* **64**, 104-120 (2013).

307   10   Anderson, R. F. *et al.* Wind-Driven Upwelling in the Southern Ocean and the Deglacial

308   Rise in Atmospheric CO2. *Science* **323**, 1443 - 1448 (2009).

309   11   Lovenduski, N. S., Gruber, N. & Doney, S. C. Toward a mechanistic understanding of the

310   decadal trends in the Southern Ocean carbon sink. *Global Biogeochem. Cy.* **22**, n/a-n/a,

311   doi:10.1029/2007GB003139 (2008).

312   12   Purich, A., Cai, W., England, M. H. & Cowan, T. Evidence for link between modelled

313   trends in Antarctic sea ice and underestimated westerly wind changes. *Nat. Commun.* **7**,

314   10409, doi:10.1038/ncomms10409,

315   http://www.nature.com/articles/ncomms10409#supplementary-information (2016).

316   13   Wanninkhof, R. *et al.* Global ocean carbon uptake: magnitude, variability and trends.

317   *Biogeosciences* **10**, 1983-2000, doi:10.5194/bg-10-1983-2013 (2013).

318   14   Kilian, R. & Lamy, F. A review of Glacial and Holocene paleoclimate records from

319   southernmost Patagonia (49–55°S). *Quaternary Sci. Rev.* **53**, 1-23,

320   doi:http://dx.doi.org/10.1016/j.quascirev.2012.07.017 (2012).

321   15   Fontana, S. L. & Bennett, K. Postglacial vegetation dynamics of western Tierra del Fuego.

322   *Holocene* **22**, 1337-1350, doi:doi:10.1177/0959683612444144 (2012).

323   16   Waldmann, N. *et al.* Integrated reconstruction of Holocene millennial-scale

324   environmental changes in Tierra del Fuego, southernmost South America. *Palaeogeogr.,*

325   *Palaeocl.* **399**, 294-309, doi:http://dx.doi.org/10.1016/j.palaeo.2014.01.023 (2014).

326   17   Moy, C. M. *et al.* Isotopic Evidence for Hydrologic Change Related to the Westerlies in

327   SW Patagonia, Chile During the Last Millennium. *Quaternary Sci. Rev.* **27**, 1335-1349

328   (2008).

329   18   .Bertrand, S., Hughen, K., Sepúlveda, J. & Pantoja, S. in *Supplement to: Bertrand, S et al.*

330   *(2014): Late Holocene covariability of the southern westerlies and sea surface*

331   *temperature in Northern Chilean Patagonia. Quaternary Sci. Rev., 105, 195-208,*

332   *doi:10.1016/j.quascirev.2014.09.021*   (PANGAEA, 2014).

333   19   Lamy, F. *et al.* Antarctic Timing of Surface Water Changes off Chile and Patagonian Ice

334   Sheet Response. *Science* **304**, 1959 - 1962 (2004).

335   20   Strother, S. L. *et al.* Changes in Holocene vegetation, climate and the intensity of

336   Southern Hemisphere Westerly Winds based on a high-resolution palynological record

337   from sub-Antarctic South Georgia. *Holocene* **25**, 263-279 (2015).

338   21   Turney, C. S. M. *et al.* A 250-year periodicity in Southern Hemisphere westerly winds

339   over the last 2600 years. *Clim. Past* **12**, 189-200, doi:10.5194/cp-12-189-2016 (2016).

340   22   Vanneste, H. *et al.* Late-glacial elevated dust deposition linked to westerly wind shifts in

341   southern South America. *Sci. Rep.* **5, 11670, doi:10.1038/srep11670** (2015).

342   23   Sime, L. C. *et al.* Sea ice led to poleward-shifted winds at the Last Glacial Maximum: the

343   influence of state dependency on CMIP5 and PMIP3 models. *Clim. Past* **12**, 2241-2253,

344   doi:10.5194/cp-12-2241-2016 (2016).

345   24   Australian-Government-Bureau-of-Meterology. *Climate statistics for Australian locations,*

346   *Macquarie Island*,

347   <http://www.bom.gov.au/climate/averages/tables/cw_300004_All.shtml> (2017).

348   25   Saunders, K. M., Hodgson, D. A. & McMinn, A. Quantitative relationships between

349   benthic diatom assemblages and water chemistry in Macquarie Island lakes and their

350   potential to reconstruct past environmental changes. *Antarct. Sci.* **21**, 35-49,

351   doi:10.1017/S0954102008001442 (2009).

352 26   Röthlisberger, R. *et al.* Dust and sea salt variability in central East Antarctica (Dome C)

353   over the last 45 kyrs and its implications for southern high-latitude climate. *Geophys.*

354   *Res. Lett* **29**, 24-21-24-24, doi:10.1029/2002GL015186 (2002).

355 27   Xiao, W., Esper, O. & Gersonde, R. Last Glacial - Holocene climate variability in the

356   Atlantic sector of the Southern Ocean. *Quaternary Sci. Rev.* **135**, 115-137,

357   doi:http://dx.doi.org/10.1016/j.quascirev.2016.01.023 (2016).

358 28   Ferry, A. J. *et al.* First records of winter sea ice concentration in the southwest Pacific

359   sector of the Southern Ocean. *Paleoceanography* **30**, 1525-1539,

360   doi:10.1002/2014PA002764 (2015).

361 29   Bianchi, C. & Gersonde, R. Climate evolution at the last deglaciation: the role of the

362   Southern Ocean. *Earth Planet. Sc. Letters* **228**, 407-424,

363   doi:http://dx.doi.org/10.1016/j.epsl.2004.10.003 (2004).

364 30   Jouzel, J. *et al.* Orbital and Millennial Antarctic Climate Variability over the Past 800,000

365   Years. *Science* **317**, 793-796, doi:10.1126/science.1141038 (2007).

366 31   Masson, V. *et al.* Holocene climate variability in Antarctica based on 11 ice-core isotope

367   records. *Quaternary Res.* **54**, 348-358 (2000).

368 32   Fletcher, M.-S. & Moreno, P. I. Zonally symmetric changes in the strength and position

369   of the Southern Westerlies drove atmospheric CO_2 variations over the past 14 k.y.

370   *Geology* **DOI: 10.1130/G31807.1** (2011).

371   33   Moreno, P. I. *et al.* Onset and Evolution of Southern Annular Mode-Like Changes at

372   Centennial Timescale. *Sci. Rep.* **8**, 3458, doi:10.1038/s41598-018-21836-6 (2018).

373   34   Prebble, J.G.. *et al.* Evidence for a Holocene Climatic Optimum in the southwest Pacific:

374   A multiproxy study. *Paleoceanography* **32**, 763-779, doi:doi:10.1002/2016PA003065

375   (2017).

376   35   Röthlisberger, R. in *Data Contribution Series #2005-046*   (ed IGBP PAGES/World Data

377   Center for Paleoclimatology) (NOAA/NGDC Paleoclimatology Program, Boulder CO, USA,

378   2005).

379   36   Monnin, E. *et al.* Atmospheric CO_2 Concentrations over the Last Glacial Termination.

380   *Science* **291**, 112-114, doi:10.1126/science.291.5501.112 (2001).

381   37   Brovkin, V. *et al.* Comparative carbon cycle dynamics of the present and last interglacial.

382   *Quaternary Sci. Rev.* **137**, 15-32, doi:https://doi.org/10.1016/j.quascirev.2016.01.028

383   (2016).

384   38   Stocker, B. D., Yu, Z., Massa, C. & Joos, F. Holocene peatland and ice-core data

385   constraints on the timing and magnitude of CO_2 emissions from past land use. *P. Natl. A.*

386   *Sci.* **114**, 1492-1497, doi:10.1073/pnas.1613889114 (2017).

387   39   Saunders, K. M. *et al.* Ecosystem impacts of feral rabbits on World Heritage sub-

388   Antarctic Macquarie Island: A palaeoecological perspective. *Anthropocene* **3**, 1-8 (2013).

389   40   Bracegirdle, T. J., Hyder, P. & Holmes, C. R. CMIP5 Diversity in Southern Westerly Jet

390   Projections Related to Historical Sea Ice Area: Strong Link to Strengthening and Weak

391   Link to Shift. *J.. Climate* **31**, 195-211, doi:10.1175/jcli-d-17-0320.1 (2018).

392   41   Wolff, E. W. *et al.* Southern Ocean sea-ice extent, productivity and iron flux over the

393   past eight glacial cycles. *Nature* **440**, 491-496 (2006).

394   42   Bracegirdle, T. J. *et al.* Assessment of surface winds over the Atlantic, Indian, and Pacific

395   Ocean sectors of the Southern Ocean in CMIP5 models: historical bias, forcing response,

396   and state dependence. *J. Geophys. Res.-Atmos.* **118**, 547-562, doi:10.1002/jgrd.50153

397   (2013).

398   43   Peter, K., Hubertus, F., Guy, M. & E., Z. R. Quantitative interpretation of atmospheric

399   carbon records over the last glacial termination. *Global Biogeochem. Cy.* **19**,

400   doi:doi:10.1029/2004GB002345 (2005).

401   44   Chavaillaz, Y., Codron, F. & Kageyama, M. Southern westerlies in LGM and future

402   (RCP4.5) climates. *Clim. Past* **9**, 517-524, doi:10.5194/cp-9-517-2013 (2013).

403   45   Rojas, M. Sensitivity of Southern Hemisphere circulation to LGM and 4 × CO2 climates.

404   *Geophys. Res. Lett.* **40**, 965-970, doi:10.1002/grl.50195 (2013).

405   46   Van Nieuwenhuyze, W. *Reconstruction of Holocene paleoenvironmental changes in the*

406   *sub-Antarctic region* PhD thesis, University of Ghent, (2015).

407   47   Davies, S. J., Lamb, H. F. & Roberts, S. J. in *Micro-XRF Studies of Sediment Cores,*

408   *Developments in Palaeoenvironmental Research series,* (eds Croudace IW & Rothwell

409   RG) (Springer, 2015).

410   48   Heimburger, A., Losno, R., Triquet, S. & Nguyen, E. B. Atmospheric deposition fluxes of

411   26 elements over the Southern Indian Ocean: Time series on Kerguelen and Crozet

412   Islands. *Global Biogeoch. Cy.* **27**, 440-449, doi:10.1002/gbc.20043 (2013).

413   49   Butz, C. *et al.* Hyperspectral imaging spectroscopy: A promising method for the

414   biogeochemical analysis of lake sediments. *J. Appl. Remote Sens.* **9**,

415   doi:10.1117/1111.JRS.1119.096031 (2015).

416

431   **Author contributions**

432   DH, KS and SR contributed equally to this work. Fieldwork was carried out by KS, DH, SR, WVN.

433   Analytical work was performed by SR (micro-XRF, sedimentology, chronology, statistical

434   analyses) and SD (micro-XRF), KS and BP (D-I conductivity analyses, chronology, sedimentology),

435   WVN (fieldwork, diatom analysis), KS, CB and MG (hyperspectral imaging) and LS (modelling).

436   DH, KS, SR and BP wrote the manuscript and supplementary information with input from all

437   authors.

438

439   **Competing Interests statement:** The authors declare no competing financial interests

440

441   **Figure captions**

442

443   **Figure 1. Southern Hemisphere westerly winds and wind anomalies in relation to the location**

444   **of Macquarie Island (white circle) a**. Location of Macquarie Island in the Southern Ocean within

445   the core of the Southern Hemisphere Westerly wind (SHW) belt. White square = EPICA Dome C

446   ice core (EDC). Grey triangle = marine core PS2090, white triangle = marine core E27-23; SHW =

447   Southern Hemisphere Westerlies, PF = Polar Front, SACCF = Southern Antarctic Circumpolar

448   Current Front. **b.** Location of Macquarie Island and Emerald Lake (pansharpened LANDSAT8

449   satellite image, bands 4,3,2). **c.** Annual mean and **d.** Decadal wind speed anomalies associated

450   with the top 20% of highest wind speed events at Macquarie Island (see Supplementary Notes 1

451   and 2 for details).

452

453   **Figure 2. Changes in relative strength of the Southern Hemisphere westerly winds based on**

454   **proxies in a sediment core from Emerald Lake. a.** Diatom-inferred (D-I) conductivity. **b.**

455   Titanium (Ti) micro-XRF analysis. **c.** Micro-XRF Principal Components Analysis Axis 1. **d.**

456   Hyperspectral ratios (R_{850}/R_{900}). Red lines = 100-year interval 2nd order LOESS-smoothing.

457 Periods of increased wind strength defined as > than the 95% upper bound of the mean (blue

458 horizontal lines; see Supplementary Note 5 and Supplementary Table 6). Green shading

459 indicates when proxies compromised by erosional inputs from non-indigenous species [42]. LGIT =

460 Last Glacial–Interglacial Transition, EH = early Holocene, MH = mid Holocene, LH = late

461 Holocene. Horizontal bar = formal EH. Lithology described in Supplementary Table 3 and Note 4.

462

463 **Figure 3. Comparison of Macquarie Island wind proxies with sea ice, temperature and CO_2 a.**

464 Diatom-inferred (D-I) conductivity **b.** Titanium (Ti) micro-XRF data. **c.** Southern Ocean winter

465 sea ice concentration (WSIC) from marine cores PS2090 [29] and E27-23 [30]. **d.** EPICA Dome C sea

466 salt Na^+ aerosol flux (representing new sea ice surfaces) [38]. **e.** EPICA Dome C temperature
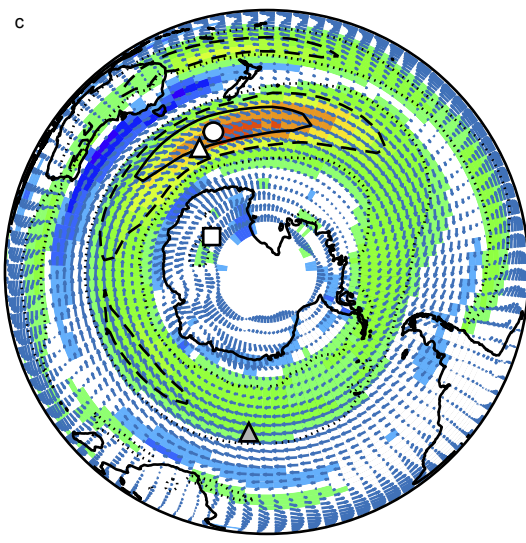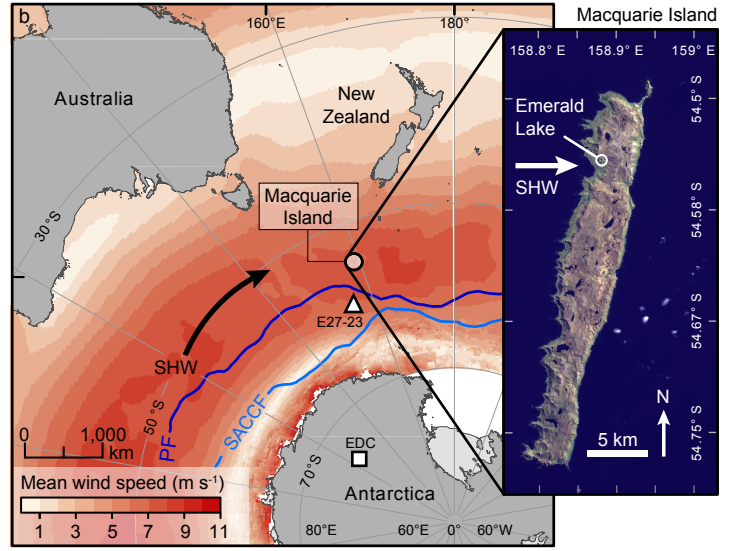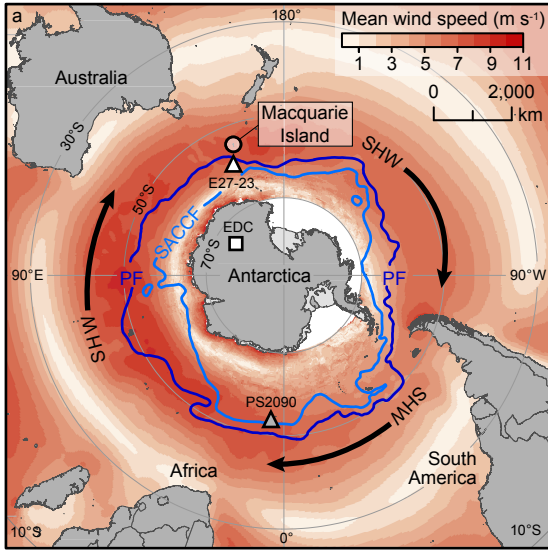
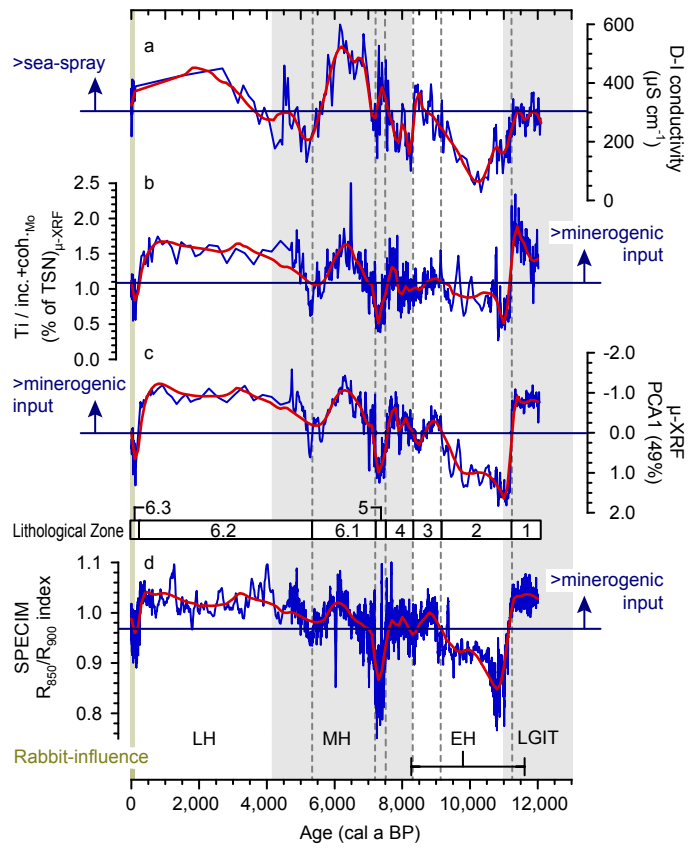467 anomaly [32]. **f.** EPICA Dome C CO_2 [39]. Grey dotted lines are lithological zones defined in Figure 2.

468 Orange highlights periods when above-mean winds correspond to increasing CO_2, blue when

469 below-mean winds correspond to decreasing CO_2. LGIT = Last Glacial–Interglacial Transition, EH

470 = early Holocene, MH = mid Holocene, LH = late Holocene. Horizontal bar = formal EH.

471

Rabbit-influence

a
D-I conductivity (μS cm^{-1})
600
400
200
0

b
Ti / inc.+coh. (% of TSN)$_{μ-XRF}$,$_{Mo}$
2.5
2.0
1.5
1.0
0.5
0.0
Mean

c
Southern Ocean WSIC %
S. Atlantic PS2090
60
40
20
0

S. Pacific E27-23
60
40
20
0

d
EDC Na$^+$ flux (ng cm^{-2} yr^{-1})
90
80
70
60
50
40
30

e
EDC Temp. (°C)
4
2
0
-2
-4
-6

f
EDC CO$_2$ (ppm)
280
260
240
220

LH   MH   EH   LGIT

Age (cal a BP)
0   2,000   4,000   6,000   8,000   10,000   12,000